Evolution of thermal electron distributions in the magnetotail: convective heating and scattering-induced losses

P. I. Shustov [1,2], A. S. Lukin[1,2], X.-J. Zhang[3], A. V. Artemyev[1,3], A. A. Petrukovich[1], V. Angelopoulos[3]

[1]Space Research Institute, Russian Academy of Sciences, Moscow, Russia
[2]Faculty of Physics, National Research University Higher School of Economics, Moscow, Russia.
[3]Department of Earth, Planetary, and Space Sciences, University of California, Los Angeles, California, USA

Key Points:

- We compared thermal electron spectra observed simultaneously at different radial distances
- Our results indicate that adiabatic heating alone significantly overestimates the observed electron energization
- Electron losses at the strong diffusion limit are required to describe the evolution of electron fluxes along different radial distances

Corresponding author: Pavel Shustov, p.shustov@cosmos.ru

Abstract

Earth's magnetotail is filled with solar wind and ionospheric electrons, whose initial energies are significantly lower than the typical energies (temperatures) of plasmasheet electrons. One of the most common mechanisms responsible for heating of solar wind and ionospheric electrons in Earth's magnetotail is adiabatic heating caused by earthward convection of these electrons from the deep tail (i.e., from the region of a weak magnetic field) towards the region of stronger magnetic fields closer to Earth. This heating is moderated by electron losses into the ionosphere due to local wave scattering. In this study, we compare electron spectra from simultaneous observations of The Time History of Events and Macroscale Interactions during Substorms (THEMIS) spacecraft at different radial distances with spectra obtained from a simple model that includes adiabatic heating and losses. Our comparison shows that the model heating significantly overestimates the increase in energetic (> 1 keV) electron fluxes, indicating that losses are essential for accurate modelling of the observed spectra. The required electron losses are similar to or even greater than the losses in the strong diffusion limit (when the loss cone is full). The latter can be interpreted as loss cone widening by field-aligned electron acceleration.

1 Introduction

Magnetotail electrons contribute significantly to current sheet formation (e.g., Artemyev et al. (2020)) and play a crucial role in magnetosphere-ionosphere coupling via precipitation (e.g., (Newell et al., 2009; Khazanov et al., 2018; Ni et al., 2016; Nishimura et al., 2020)) and field-aligned currents (e.g., Chaston et al. (2005); Keiling et al. (2009)). Magnetotail electron energization and dynamics are determined by the interplay between their various sources and heating mechanisms. Three main sources of magnetotail electrons are: solar-wind electrons transported from the distant tail (Sergeev et al., 1996; Ganushkina et al., 2013); electrons transported from the ionosphere (Walsh et al., 2013); and magnetosheath electrons transported across the low-latitude magnetopause (Fujimoto et al., 1998). Three main heating mechanisms are: adiabatic heating by convection (Lyons, 1984; Sergeev et al., 2001; Artemyev et al., 2012); acceleration by magnetic reconnection (Imada et al., 2011; Egedal et al., 2012) and reconnection-related transients (e.g., dipolarization fronts, see Ashour-Abdalla et al. (2011); Gabrielse et al. (2012); Birn et al. (2013)); and acceleration by transient parallel electric fields carried by kinetic Alfven waves (Damiano et al., 2015; Artemyev et al., 2015; Damiano et al., 2016). The relative contributions of all these sources and energization mechanisms are still unclear. Unlike other mechanisms, which are transient, the first mechanism operates continuously, and thus is likely the most important source of thermal electrons in the mid- and near-Earth magnetotail.

When transient acceleration is not occurring, electron heating by plasma convection should be moderated mostly by electron scattering and subsequent losses to the ionosphere. Thermal and subthermal electron scattering is commonly attributed to electron-cyclotron (Ni et al., 2012; X. Zhang et al., 2014), whistler-mode (Ni, Thorne, Meredith, et al., 2011; Panov et al., 2013; Khazanov et al., 2014; Ma et al., 2020) waves and various broadband electrostatic waves (Vasko et al., 2017; Shen et al., 2020; Khazanov et al., 2021), whereas energetic ($>$ few keV) electron scattering is attributed to magnetic field-line curvature (Birmingham, 1984; Büchner & Zelenyi, 1989). Strong currents in the magnetotail current sheet lead to a small (< 100 km) curvature field-line radius (Runov et al., 2006). Thus, even without transients traditionally associated with enhanced electron precipitation, > 1 keV electron scattering could be effective (Liang et al., 2011, 2012; Panov et al., 2013; Eshetu et al., 2018). To date, these quiet-time electron losses have not been quantified, and how they modify convective heating is unknown. Details of such combined heating/losses effect are important for accurate modeling of electron transport into the inner magnetosphere, where these electrons

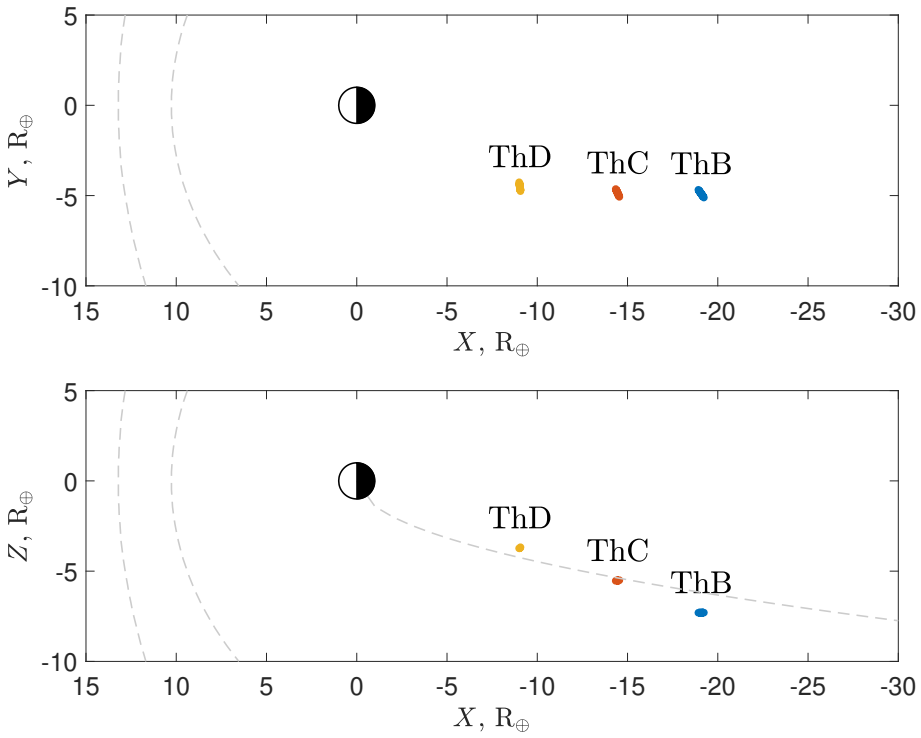

Figure 1. THEMIS spacecraft positions in GSM X-Y and X-Z planes during one event from our dataset (during a one-hour time span).

serve as the main energy source for electromagnetic whistler-mode waves (Tao et al., 2011; X. Zhang et al., 2018) as well as a source of seed electrons for the radiation belts (e.g., Gabrielse et al. (2012); Ganushkina et al. (2014, 2015); Jaynes et al. (2015)).

To investigate the evolution of thermal and suprathermal electrons during their earthward convection, one must measure their spectra simultaneously at different distances downtail of Earth. Time-averaged statistics (Stiles et al., 1978; Walsh et al., 2011; Artemyev et al., 2014) from single spacecraft missions do not allow one to separate temporal effects (caused by transient flows) from spatial effects related to electron heating due to quasi-steady transport along the tail. The THEMIS mission (Angelopoulos, 2008), however, with several spacecraft distributed along the tail, provides a unique opportunity for investigations of such evolution. Recent results from this mission show an increase in the electron temperature T_e with B_z magnetic field magnitude (in GSM coordinates) in the region of $x \in [-30, -10]R_E$ downtail (Artemyev et al., 2013; Runov et al., 2015). Although these observations are consistent with the adiabatic heating model (i.e., $T_e/B_z^q \sim const$ and $q \leq 1$, because the conservation of the electron magnetic moment and the second adiabatic invariant results in electron energy increase with the magnetic field increase along the electron drift orbits, see Tverskoy (1969); Zelenyi et al. (1990)) the absence of strong transverse anisotropy in heated electrons indicates that scattering is operating (Lyons, 1984). Therefore, electron distribution functions must be investigated to estimate the role of electron losses in the process of adiabatic heating.

We analyze measurements of three THEMIS spacecraft when they were at large separations (several to tens of Earth radii), nearly aligned along the magnetotail (along the typical direction of quasi-steady convection), around the magnetic equator (see typical spacecraft positions during one event in Fig.1). Such selected observational intervals (hereafter called "events") allow us to estimate the efficiency of adiabatic heating and the timescales of scattering that result in electron losses. We also compare these estimates to the strong diffusion limit in the magnetotail and speculate on nature of the implicated electron losses.

A detailed description of the observational dataset and event list is given in Sect. 2. In Sections 3 and 4, we provide estimates of adiabatic heating and losses as derived from the observed electron spectra during each event. In Sect. 5, we discuss possible uncertainties in our analysis caused by dawn-dusk gradients of the electron spectra in the deep tail or by local acceleration mechanisms. We also provide estimates of the altitudes at which electrons should be lost (i.e., estimates of the actual loss cone size). These estimates, which are derived from the strong diffusion equation, have lifetimes consistent with the observed electron spectra. We discuss possible mechanisms responsible for electron losses and summarize our findings in Sect. 6.

2 Spacecraft data and analysis technique

We study six events (observational intervals) during which three THEMIS spacecraft (ThB, ThC, and ThD) were in the near-equatorial magnetotail current sheet for one hour. We use magnetic field (Auster et al., 2008) measurements with 3s (spin-period) resolution in GSM coordinates. THEMIS ion and electron electrostatic analyzers (McFadden et al., 2008) provide ion flow velocity, electron moments, and energy spectra with the same resolution.

An example spacecraft alignment is shown in Fig. 1; the entire list of selected events is in Table (1). From these time intervals, we choose (for each satellite) only measurements very close to the neutral plane: with a B_x component less than B_z or $|B| < 5$nT (i.e., the field magnitude is small enough). To exclude very fast crossings of the current sheet (which could be prone to temporal aliasing of the plasma mea-

Table 1. Table of events

Number	Date	Start time	End time
1.	01-Jan-2008	05:00	05:30
2.	01-Jan-2008	08:30	09:30
3.	17-Jan-2008	08:20	08:50
4.	26-Feb-2008	05:10	05:30
5.	14-Jan-2009	10:00	10:30
6.	14-Jan-2009	12:00	12:30

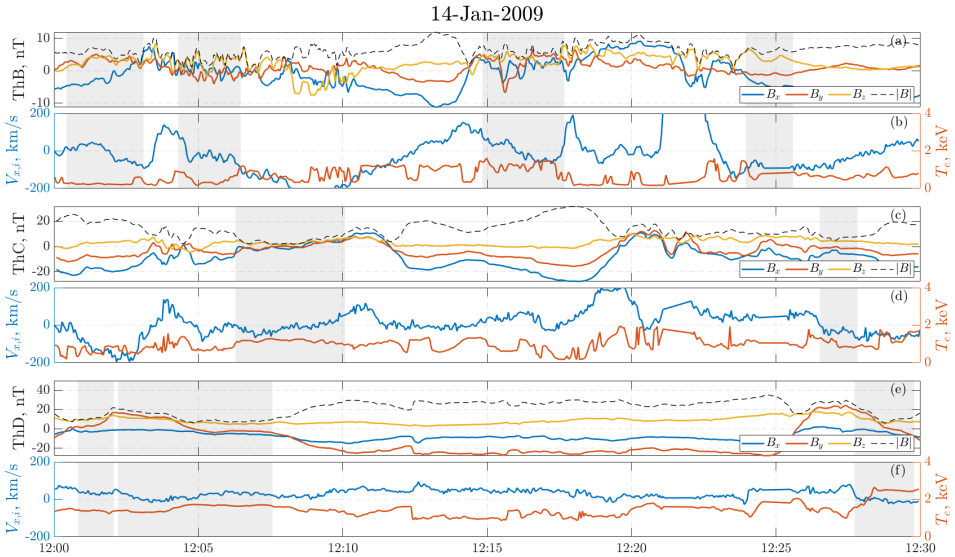

Figure 2. An event from our dataset. Panels (a), (c), and (e) show magnetic field measurements from FGM at ThB, ThC, and ThD; panel (b), (d), and (f) show ion velocity (v_x GSM) and electron temperature measured by the three spacecraft. The gray boxes mark selected time intervals when the satellite is close enough to the current layer according to our criteria in Sect. 2.

surements), we retain only subintervals with continuous measurements longer than one minute. In addition, we exclude subintervals that contain dipolarization events (Runov et al., 2009) in the downtail region: if $B_z > 15$ nT on ThB or ThC, we exclude ± 5 min measurements around this strong B_z.

One event from Table (1) is shown in Figure 2. The three pairs of panels show magnetic field (GSM components and magnitude), v_x component of ion bulk flow, and electron temperature measurements from the three spacecraft (ThB was $\sim 20R_E$ downtail, ThC was $\sim 15R_E$ downtail, and ThD was $\sim 10R_E$ downtail). During several subintervals (shown by grey background) the spacecraft were sufficiently close to the equator to consider differences of their electron measurements as a result of different spacecraft radial distances. We identify $|v_x| > 100$km/s as a fast flow (Angelopoulos et al., 1993, 2008) and do not take measurements within such fast flows into consideration. In the event from Fig.2, ThD does not observe any fast flows, and we exclude ThC, ThB measurements with such flows (note that the midtail is generally filled with fast flows

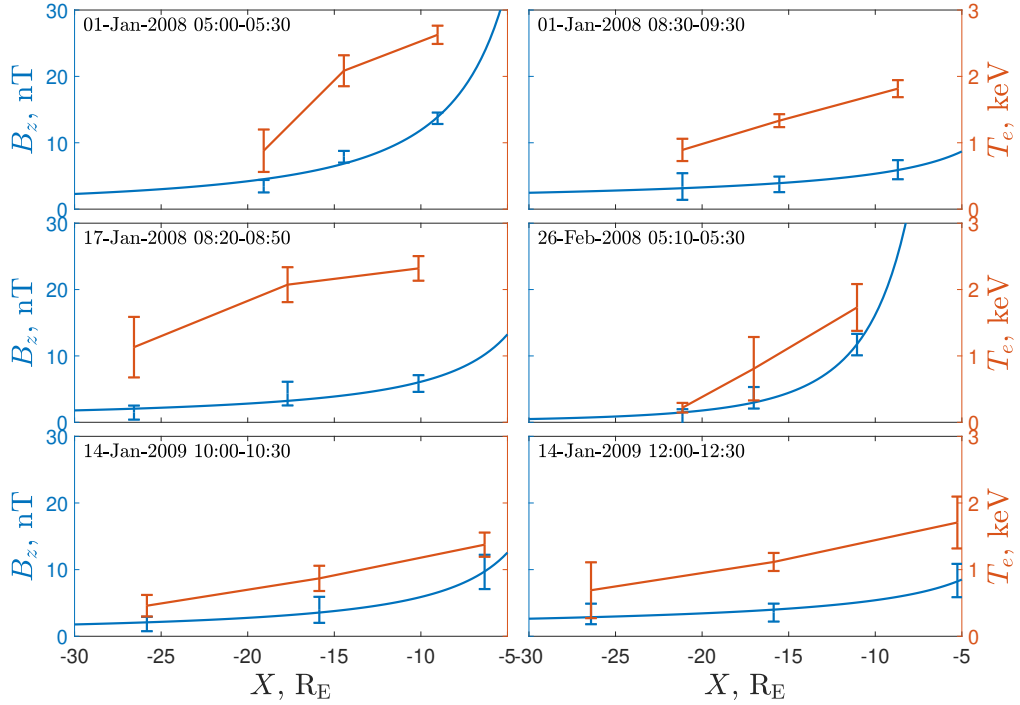

Figure 3. Error bars show the electron temperature $T_e(x)$ and the magnetic field $B_z(x)$ during the six events from Table (1) at ThB, ThC and ThD possitions with time averaging over near-current-sheet subintervals for each event (see text for details). Blue curve corresponds to power-law fit obtained by least squares method.

from the distant (Kiehas et al., 2018) and near-Earth (Baker et al., 1996) reconnection regions, and such flows, usually accompanied by B_z peaks, can significantly change the electron temperature T_e and the electron spectrum (Gabrielse et al., 2014; Runov et al., 2011)). The slowest temperature variations are caused by the spacecraft's motion relative to the equator (T_e peaks at $B_x \sim 0$ and goes down as $|B_x|$ increases, see Artemyev, Zelenyi, et al. (2011)). Note that temperature variations due to energetic electron transport by fast plasma flows(Gabrielse et al., 2017, 2019) are excluded from the analysis. Thus, only observations of quiet, near-equatorial current sheet (subintervals) are selected for each event in Table (1); we evaluate the average electron temperature and B_z for these subinterval observations.

All six events are characterized by monotonic increases in the average electron temperature $T_e(x)$ and average magnetic field $B_z(x)$ (see Fig. 3). Such increases show that the selected intervals of T_e, B_z are sufficiently quiet and do not contain transients that would change the positive dT_e/dx, dB_z/dx gradients.

Figure 3 shows electron temperature and magnetic field B_z measurements at three radial distances (for B_z we also show power-law fit determined from the least square method). T_e profiles demonstrate electron heating with earthward convection. To model this heating, we analyze electron energy distributions (phase space density versus energy). We examine only energy distributions (spectra) of equatorial electrons (with pitch angles $\alpha \in [80°, 110°]$) measured near the neutral plane (see criteria in Sect. 2).

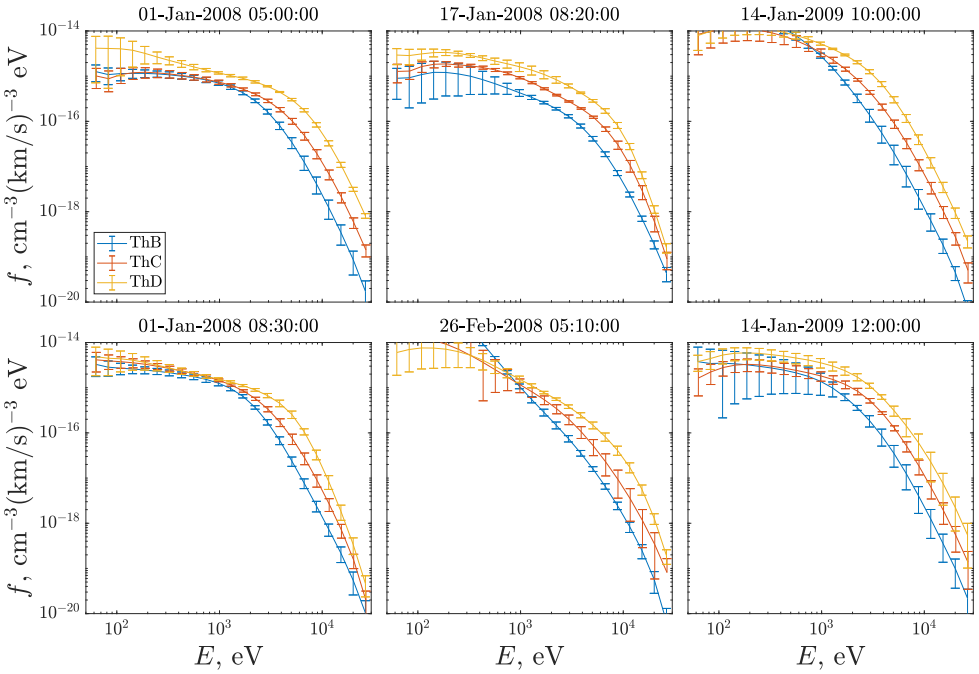

Figure 4. Electron distribution functions from the three THEMIS spacecraft during the six events, in our database (see text for details).

The distribution functions averaged over the selected time intervals are shown in Fig. 4. To exclude cold ionospheric electrons and possible photoelectrons in the lower energies, we exclude measurements in the $E < 50$ eV energy range. We examine the phase space density that is expected to be conserved (in the absence of electron losses) along electron drift orbits. The distribution functions shown in Fig. 4 have a flat energy profile extended over a broad energy range for $E < 1$ keV (such a profile is sometimes called a flat-top distribution, see Asano et al. (2008); Nagai et al. (2013)). For $E > 1$ keV the phase space density drops exponentially (or as a power law, see Christon et al. (1991); Sarafopoulos et al. (2001)). This profile is typical of electron spectra in the magnetotail current sheet (see statistics in Artemyev et al. (2014)).

We also examine the electron flux anisotropy for all events. Figure 5 shows that the normalized flux difference $(f_{\parallel} - f_{\perp})/(f_{\parallel} + f_{\perp})$ (where $f_{\parallel,\perp}$ are the average fluxes over $[0, 30°], [150°, 180°]$ and $[75°, 105°]$ pitch angles) is larger than one for $E < 1$ keV. This field-aligned anisotropy of < 1 keV electrons is typical in the Earth's magnetotail (Walsh et al., 2011; Artemyev et al., 2014) and can be associated with the ionospheric outflow (Walsh et al., 2013). In the energy range of > 1 keV, $(f_{\parallel} - f_{\perp})/(f_{\parallel} + f_{\perp})$ is rather close to zero. Thus, we can assume that pitch-angle scattering is sufficiently strong for this energy range.

3 Electron convective heating

Assuming adiabatic electron heating along electron drift orbits (during earthward convection), we can compare the phase space density profiles measured by ThB and map profiles measured by ThC and ThD (which are closer to Earth) to the location of ThB. Figure 6 (right) shows such a comparison for one event on 1 January 2008. The phase space density measured at ThB clearly overestimates the phase space density recalculated at ThB from ThC and ThD, i.e., to obtain spectra observed by ThC

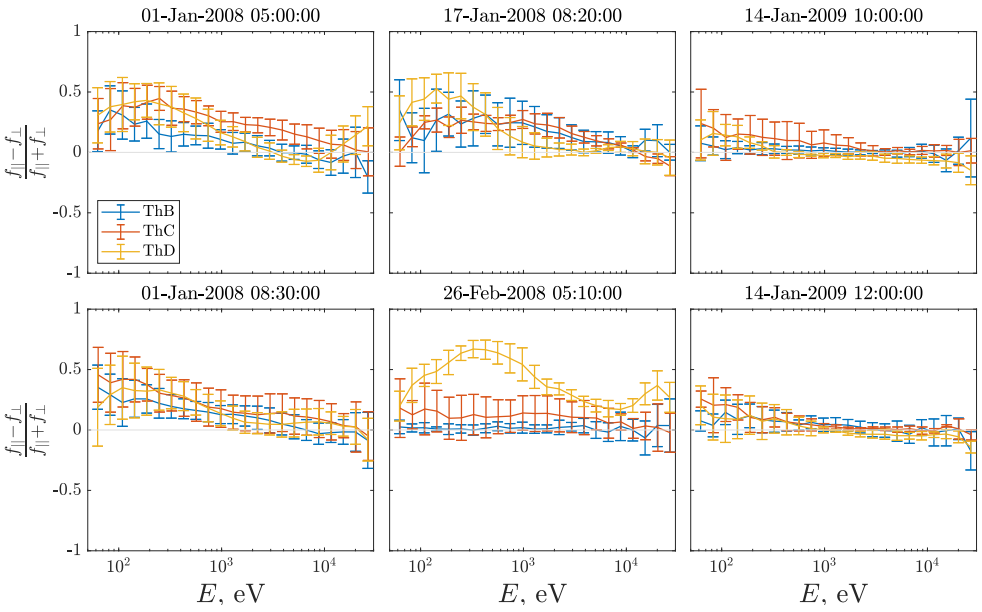

Figure 5. Electron distribution functions from three spacecraft during six events. See text for details.

and ThD from ThB, we should start with phase space density magnitudes smaller than actual measuremebrs on ThB. Therefore, Fig. 6 shows that the evolution of electron distributions (during earthward electron convection) is most likely affected by electron losses. Note that for this spectrum comparison, we use omnidirectional electron fluxes, because Fig. 5 demonstrates almost isotropic electron distributions at > 1 keV energies.

And, indeed, several mechanisms responsible for electron scattering result in pitch-angle decrease and finally in losses into the atmosphere from, for example, resonant electron interactions with electron cyclotron harmonic waves (X. Zhang et al., 2014; X.-J. Zhang et al., 2015), with whistler waves (Ni, Thorne, Meredith, et al., 2011; Khazanov et al., 2014), electrostatic turbulence (Vasko et al., 2017; Shen et al., 2020; Khazanov et al., 2021) or electron scattering by magnetic field line curvature (Birmingham, 1984). The latter one can be significantly enhanced by ultra-low-frequency B_z fluctuations in the midtail (Volwerk et al., 2004), which locally reduce equatorial B_z and decrease the curvature radius (Eshetu et al., 2018). The large variety of scattering/loss mechanisms suggests that such losses in 2D energy, pitch-angle space can only be investigated quantitatively by combining global MHD simulations (e.g., Eshetu et al. (2018)) with evaluations of wave-particle interaction (e.g., Ni et al. (2016); Khazanov et al. (2018)). Here we simplify the description of losses and combine all them within a lifetime estimate that describes how phase space density decreases with time for different electron energies (see details of this approach in Horne et al. (2005); Balikhin et al. (2012)).

To determine whether a combination of adiabatic heating and losses can reproduce the observed evolution of the electron energy distribution, $f(\mathcal{E})$, we use a simple kinetic equation:

$$\frac{\partial f}{\partial t} = \frac{\partial f}{\partial \mathcal{E}}\dot{\mathcal{E}} - \frac{f}{\tau_{loss}(\mathcal{E})} \tag{1}$$

where $\tau_{loss}(\mathcal{E})$ is a characteristic electron loss time, and $\dot{\mathcal{E}}$ is the energy change due to earthward convection. Assuming an adiabatic energy change, $\mathcal{E} = \mathcal{E}_0 b^q$, $b = B_z/B_{z0}$,

we write $\dot{\mathcal{E}} = q\mathcal{E}_0 b^{q-1} (\partial b/\partial x)\, \dot{x}$, where q may vary between one (for anisotropic heating of equatorial electrons, see Tverskoy (1969)) and 2/3 (for heating accompanied by isotropization due to pitch-angle scattering, see Lyons (1984)). Electrons drift toward Earth with $\dot{x} = V(x) = cE_y/B_z(x)$ speed and convection electric field $E_y \approx const$ (Sergeev et al., 1996). Thus, we can write:

$$\dot{\mathcal{E}} = q\mathcal{E}_0 b^{q-1} \frac{1}{B_{z0}} \frac{\partial B_z}{\partial x} c \frac{E_y}{B_z} = q\mathcal{E} c \frac{\partial B_z}{\partial x} \frac{E_y}{B_z^2} \equiv \frac{\mathcal{E}}{T(x)} \tag{2}$$

where $T(x)$ is the timescale of energy change due to adiabatic heating.

Therefore, we obtain the modified kinetic equation as follows:

$$\frac{\partial f}{\partial x} = \frac{\partial f}{\partial \mathcal{E}} \frac{\mathcal{E}}{l(x)} - \frac{1}{V(x)} \frac{f}{\tau_{loss}(\mathcal{E})} \tag{3}$$

where $l(x) = T(x)V(x) = (q\partial \ln B_z/\partial x)^{-1}$.

For infinitely large τ_{loss} (i.e., in absence of losses), this equation describes adiabatic heating that is shown to result in overestimation of the phase space density increase for energetic electrons (see Fig. 6). Thus, we introduce a finite τ_{loss} for energetic electrons ($\mathcal{E} > \mathcal{E}_*$) that can be scattered into a loss cone by magnetic field-line curvature (Eshetu et al., 2018) and wave-particle interactions (Ni et al., 2016):

$$\tau_{loss}^{-1} = \begin{cases} 0, & \text{if } \mathcal{E} < \mathcal{E}_* \\ \tau_0^{-1}(\mathcal{E}/\mathcal{E}_* - 1)^{\beta}, & \text{if } \mathcal{E} > \mathcal{E}_* \end{cases} \tag{4}$$

This function depends on three parameters: β, τ_0 and $\mathcal{E}_*$. We determine their values by matching the kinetic equation solution to the observed evolution of the electron energy distribution in the following way. We start from the time-averaged (during the subintervals near the neutral plane for each event) distribution function measured by THEMIS B $f_B(\mathcal{E})$ (farthest from Earth) and substitute it into Equation (3) as a initial condition. Then we obtain solution of this equation for x corresponding to the locations of THEMIS D (i.e., $f_{B\to D}(\mathcal{E})$). Towards that goal we use the magnetic field $B_z(x)$ profile (obtained from fitting the observed magnetic field by a power-law function by least squares method, see Fig.3). Additionally, we use a constant electric field E_y (we set $E_y = 0.2$ mV/m as typical of quiet-time magnetotail convection (Angelopoulos et al., 1993); note that the magnitude of E_y does not change the efficiency of electron adiabatic heating, which is controlled by the $B_z(x)$ profile). We define β, τ_0 and $\mathcal{E}_*$ by least squares method that provide the best agreement between solution of Equation (3) – $f_{B\to D}(\mathcal{E})$, and the observed electron energy distribution – $f_D(\mathcal{E})$. The final parameters during each event are shown in Table (2). Typical energies at which losses should be important, $\mathcal{E} \geq 1$ keV, correspond to the suprathermal electron population, which is indeed scattered by magnetic field-line curvature and wave-particle interactions (Eshetu et al., 2018; Ni et al., 2016). The typical timescale of scattering, $\tau_0 \in [10, 30]$ min, which corresponds to diffusion rates of $D \sim 10^{-3}$ s around the loss cone, is reasonable for electron cyclotron waves (Ni et al., 2012; X. Zhang et al., 2014), upper-band chorus waves (Ni, Thorne, Shprits, et al., 2011), and broadband electrostatic turbulence (Vasko et al., 2018). Note that τ_0 is mostly determined by the rate of earthward electron transport, i.e., $\tau_0 \propto 1/E_y$ and thus τ_0, can vary with the average E_y, which is further determined by magnetotail conditions and solar wind-magnetosphere coupling (Sergeev et al., 1996).

Figure 7 shows spectra $f_D(\mathcal{E})$ (blue line) and the solution of Equation (3) $f_{B\to D}(\mathcal{E})$ without any losses, which effectively corresponds to $\tau_{loss} \to \infty$ case (red line) and with τ_{loss} (yellow line) from Table (2). The high phase space density of $f_{B\to D}(\mathcal{E})$ at low energies (less than $\sim$ 1keV) results from heating of low-energy electrons (energies below $\sim$ 50eV in $f_B(\mathcal{E})$). This electron population is affected by field-aligned electric fields

Table 2. Table of τ_{loss} parameters obtained by the least squares method. The $\pm$ shows the range of parameter variation within 50% increase of the magnitude of the least squares residual.

Event	β	τ_0 (min)	$\mathcal{E}_*$ (keV)
1.	0.78 ± 0.02	214 ± 16	1.43 ± 0.10
2.	1.02 ± 0.09	23 ± 2	6.45 ± 0.30
3.	0.64 ± 0.03	13 ± 0.6	5.68 ± 0.09
4.	0.60 ± 0.32	19 ± 6.5	2.92 ± 1.43
5.	0.38 ± 0.13	51 ± 8.5	2.22 ± 0.61
6.	0.40 ± 0.02	27 ± 1.5	1.83 ± 0.11

(both quasi-static fields (Lysak & Song, 2011; Egedal et al., 2012) and wave fields (Chaston et al., 2012; Damiano et al., 2015; Artemyev et al., 2015)), and we do not describe the dynamics of this population here.

For the energy range > 1 keV, the adiabatic heating significantly overestimates the observed population of energetic electrons $f_D(\mathcal{E})$, but inclusion of the losses makes $f_{B\to D}(\mathcal{E})$ close to $f_D(\mathcal{E})$. Comparing $f_D(\mathcal{E})$ and $f_{B\to D}(\mathcal{E})$ without losses, we see that adiabatic heating not only overestimates the energetic electron phase space density, but also leads to an energy slope different from the observed one. Thus, even by altering the efficiency of heating (see discussion in Artemyev, Petrukovich, et al. (2011)), we cannot describe $f_D(\mathcal{E})$ by $f_{B\to D}(\mathcal{E})$ without losses that are more effective for higher energies (per Eq. (4)) and can change the energy spectrum slope. Comparisons of $f_D(\mathcal{E})$ (blue line) and $f_{B\to D}(\mathcal{E})$ with losses (dashed yellow line) show that our estimates of τ_0 are rather reasonable. We then compare these estimates with the maximum possible losses to the atmosphere at the strong diffusion limit.

4 Electron losses

Figure 7 compares electron spectra measured by ThD (blue) and map of ThB spectra to the ThD location by the kinetic equation solution without losses (red) and with losses (yellow). Results of this comparison clearly show the importance of electron losses in shaping the electron energy spectra during earthward convection. Estimates of $\tau_{loss}(\mathcal{E})$ can be compared with the strong diffusion limit, $\tau_{SD} = \tau_b/4\Delta\alpha_{LC}^2$ (Kennel, 1969) (where $\tau_b/4$ is a quarter of the electron full bounce period; $\Delta\alpha_{LC}$ is the loss cone size). The strong diffusion time determines the fastest possible timescale of electron losses when the loss cone remains filled due to rapid pitch-angle diffusion. Thus, the characteristic loss time τ_{loss} determined from the model/observational spectra comparison cannot be larger than this strong diffusion limit: $\tau_{loss} \geq \tau_b/4\Delta\alpha_{LC}^2$.

The electron bounce time is determined by the magnetic field profile $B(s)$:

$$\tau_b(\mathcal{E}) = \sqrt{\frac{m_e}{2\mathcal{E}}} \int_0^{s_{max}} \frac{ds}{\sqrt{1 - \sin^2 \alpha_{LC} B(s)/B_0}} \equiv \sqrt{\frac{m_e}{2\mathcal{E}}} g(\alpha_{LC}; B(s)) \tag{5}$$

and we use empirical models to calculate $\tau_b(\mathcal{E})$. Then we solve the equation

$$\tau_{loss}(\mathcal{E}) \sqrt{\frac{2\mathcal{E}}{m_e}} = \frac{g\left(\alpha_{LC}; B(s)\right)}{4\alpha_{LC}^2} \tag{6}$$

to determine the minimum α_{LC} required to explain the estimated τ_{loss}. A wider loss cone than expected from the electron losses at ~ 100 km altitude indicate on electrons

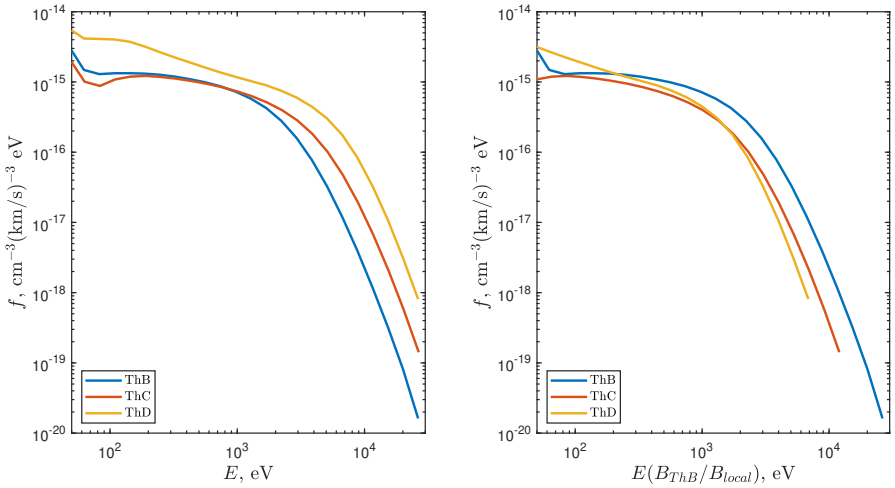

Figure 6. Observed electron distribution functions at three spacecraft (left). The same electron distribution functions energy-shifted by the adiabatic heating factor to ThB (right).

losses at higher altitudes, e.g., due to a field-aligned potential drop that alters electron dynamics at low altitudes. To show this effect we use calculated α_{LC} to determine the altitude of expected losses, R_{LC}. Although our estimates give $\alpha_{LC}(\mathcal{E})$ and $R_{LC}(E)$, in the leading approximation the loss cone angle is determined by the magnetic field configuration and does not depend on energy. However, secondary effects (such as electron losses caused by field-line acceleration in the auroral region (Lysak, 1990)) may affect α_{LC} differently for different energies.

Figure 8 (top panels) shows $\alpha_{LC}(\mathcal{E})$ determined from Equation (6) with τ_{loss} given by Equation (4) and parameters from Table (2) for three electric field values. We determine $\alpha_{LC}(\mathcal{E})$ averages of the data in all six events. The result is obtained using the T96(Tsyganenko, 1995) magnetic field model, but we check that the TS04 (Tsyganenko & Sitnov, 2005) and T01(Tsyganenko, 2002) models lead to very similar results.

As shown in Figure 8 (top panels), $\alpha_{LC}(\mathcal{E})$ may exceed the loss cone size determined from the magnetic field model for electron losses at 100km altitude (red horizontal lines), which is less than 1° in the plasma sheet (X.-J. Zhang et al., 2015). Thus, electrons should be lost at higher altitudes, e.g., because of additional field-aligned acceleration in the auroral acceleration region (Kennel, 1969; Lysak, 1990). Using magnetic moment conservation, we thus determine the magnetic field at the altitude at which electrons are expected to be lost. Comparing this field with the magnetic field models, we determine the expected altitude of losses – R_{LC}. Figure 8(bottom panels) shows that to explain the observed equatorial phase space densities, $R_{LC} < 1.5R_E$ (< 3000 km from the Earth surface) for quiet-time convection field 0.05 mV/m estimates i.e., the effective loss cone should be wider than the one derived when 100km altitude losses are assumed. This argues in favor of electrostatic potential drops or very effective wave scattering even under quiet time conditions.

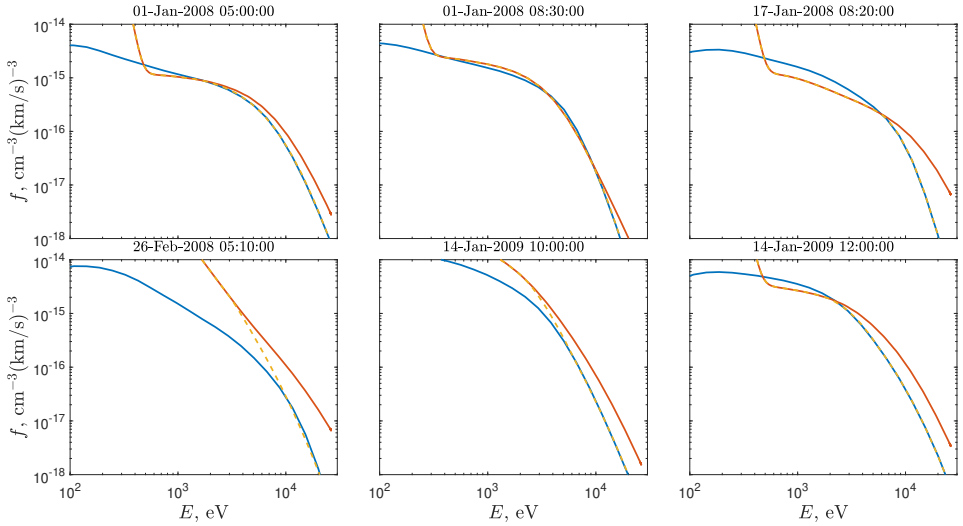

Figure 7. Comparison of electron spectra measured at ThD (blue lines) and map of ThB spectra to the ThD location for six events: red lines show maps (solutions of the kinetic equation) in the absence of electron pitch-angle scattering and accompanying losses, whereas yellow lines show maps (solutions) with these losses included.

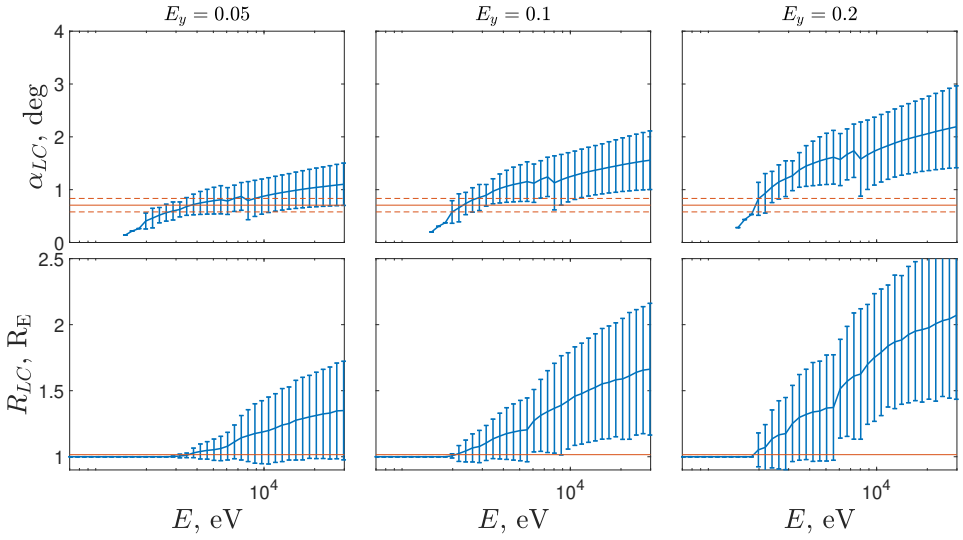

Figure 8. Blue lines with error bars show estimates of the loss-cone size needed to describe observed electron losses (top row) and radial distance R_{LC} of electron losses ($R_{LC} = R_E$ is the Earth surface and $R_{LC} < R_E$ means that required losses are weaker than the strong diffusion limit) corresponding to estimated α_{LC} (bottom row). This data averaged over a set of six events with the corresponding standard deviation shown by error bars. The solid red horizontal line in the first row shows the loss-cone angle corresponding to the ∼100km altitude (ThD magnetic field and position are used); the standard deviation is denoted by dashed red lines. The red line in the second row shows the ∼100km altitude. Three columns correspond to different magnitudes of the convection electric field E_y shown on top.

5 Discussion

Using multiple THEMIS spacecraft observations of electron energy distributions at different distances from Earth, we estimated the efficiency of adiabatic heating and required losses. Let us discuss several constraints of our approach.

5.1 Dawn-dusk gradients of electron distribution

To compare the spectra measured by THEMIS at different radial distances, we should ensure that the dawn-dusk electron drift is sufficiently weak, and all differences between spectra are caused by radial (earthward) convection, where the effects of dawn-dusk inhomogeneity are neglected (see discussion of the importance of this inhomogeneity for plasma heating on a global magnetosphere scale in Kivelson and Spence (1988)). We consider equatorial electrons ($\sim 90^\circ$ pitch angle), which drift in $\mathbf{E} = E_y \mathbf{e}_y$ and $\mathbf{B} = B(x)\mathbf{e}_z$ fields:

$$v_x = c\frac{E_y}{B_z}, \quad v_y = -c\frac{\mathcal{E}_\perp}{eB_z^2}\frac{dB_z}{dx} \tag{7}$$

where $\mathcal{E}_\perp$ is electron energy. These two drift velocity components determine the electron trajectory on the equatorial plane:

$$y - y_0 = -\frac{\mathcal{E}_{\perp,0}}{eE_y}\left(\frac{B_z}{B_{0z}} - 1\right)$$

where we use $\mathcal{E}_\perp/B_z = const$, and variables with subindex 0 are for initial electron location (i.e., at the radial distance of ThB).

Between THEMIS B ($\sim 20R_E$) and THEMIS D ($\sim 10R_E$), the magnetic field B_z typically varies from about $\sim 2-4$nT to ~ 10nT (see Fig. 3). Thus, particles with initial energy ~ 1keV at THEMIS B in $E_y = 0.1$mV/m would drift in $y - y_0 \simeq 2 \cdot 10^4$km $\simeq 3R_E$. At the radial distances of THEMIS B, there are no dawn-dusk gradients in plasma parameters with such small scales (Wang et al., 2009). Therefore, electron dawn-dusk drift most likely does not affect the electron spectrum change from THEMIS B to THEMIS D.

5.2 Local acceleration

Although the observed electron heating is generally consistent with adiabatic heating by a convection electric field, electron populations with energies below a few keV are also subject to field-aligned acceleration/cooling by parallel electric fields. In a quiet plasma sheet, however, such fields are expected to affect mostly < 1 keV electrons, for which we observe flattened electron energy spectra (see Figs. 6, 7). And, indeed, Egedal et al. (2012) demonstrated that similar flattened electron spectra can be associated with local electron acceleration by quasi-static parallel electric fields generated by ion-electron decoupling around thin current sheets (e.g., around the reconnection region). Because a finite drop in the scalar potential along magnetic field lines can accelerate electrons independently of their initial energy, the final energy distribution would have a prolonged plateau. Although there is no evidence of magnetic reconnection in THEMIS observations in the six selected events (the near-Earth reconnection is usually located around $x \sim -20 - 30R_E$ (Angelopoulos et al., 2008; Petrukovich et al., 2009; Liu et al., 2011) or even farther from Earth (Genestreti et al., 2013)), the mechanism proposed by Egedal et al. (2012) would still work well in a thin current sheet with expected finite parallel electric fields (see, e.g., (Artemyev et al., 2018)). Thus, we probably can attribute the observed flattened electron spectra at < 1 keV to the effect of such field-aligned electric fields, whereas electron heating at higher (> 1 keV) energies does not show clear field-aligned anisotropy (Artemyev et al., 2014) and is most likely associated with the adiabatic heating.

5.3 Loss cone widening

Low-altitude measurements (e.g., by DMSP (Newell et al., 2009, 2010) and FAST (Dombeck et al., 2018)) of precipitating electron fluxes generally show very high levels (around the strong diffusion limit) of fluxes from the plasma sheet. Our estimates of the required electron losses agree well with these measurements. Moreover, we suggest that the actual loss cone in the plasma sheet should widen to account for precipitation exceeding the strong diffusion estimates in our model. Such a widening can be caused by to electron acceleration along magnetic field lines at low altitudes (Mozer et al., 1980), e.g., acceleration by transient parallel electric fields of kinetic/inertial Alfven waves (Rankin et al., 1999; Chaston et al., 2002; Tikhonchuk & Rankin, 2002; Dombeck et al., 2018) or by quasi-static electric fields of the auroral acceleration region (Mozer & Kletzing, 1998; Ergun et al., 2002, 2004; Echim et al., 2009; Birn et al., 2012). Such fields are indeed observed at altitudes of a few R_E (Wygant et al., 2002; Li et al., 2014). Although such acceleration is not very important for high-energy (> 10 keV) electrons precipitating from the inner magnetosphere (Ni et al., 2016; Nishimura et al., 2020), it may significantly impact precipitation of plasma sheet energetic ($\in [1, 10]$ keV) electrons. Our results suggest that energy fluxes of plasma sheet electrons should be almost always above the strong diffusion limit (i.e., precipitating electron fluxes should be larger than fluxes uniformly filling the loss-cone determined by the magnetic field configuration), and this estimate may be important for magnetosphere-ionosphere coupling models included in global MHD simulations (e.g., El-Alaoui et al. (2008)).

5.4 Scattering mechanisms

Sufficiently strong electron pitch-angle scattering is needed to keep the loss cone filled, i.e., to provide precipitation at the strong diffusion limit. Although scattering of plasma sheet electrons is usually resonant scattering by electron cyclotron harmonic waves (Ni, Thorne, Horne, et al., 2011; X. Zhang et al., 2014; X.-J. Zhang et al., 2015), whistler-mode waves (Ni, Thorne, Meredith, et al., 2011; Ni et al., 2016; Khazanov et al., 2017), and broadband electrostatic noise (Vasko et al., 2018; Shen et al., 2020; Khazanov et al., 2021), these emissions are transient and generally associated with fast plasma flows and dipolarization fronts (Deng et al., 2010; Panov et al., 2013; X. Zhang & Angelopoulos, 2014; Malaspina et al., 2015; Mozer et al., 2015; Breuillard et al., 2016; X. Zhang et al., 2018). Steadier precipitation can be provided by curvature scattering of electrons with sufficiently large equatorial gyroradii, i.e., sufficiently large energy (Birmingham, 1984; Büchner & Zelenyi, 1989). Accurate estimates of the curvature scattering effect in stretched magnetotail field lines require precise information about the current sheet thickness L and the equatorial magnetic field component B_n transverse to the current sheet plane. These parameters can be measured only by multi-spacecraft missions (see Knetter et al. (2004); Sergeev et al. (2006) for discussions on the low accuracy of single-spacecraft measurements in determining the local coordinate system required to estimate B_n). Available magnetotail current sheet databases (Nakamura et al., 2006; Runov et al., 2006; Petrukovich et al., 2015; Vasko et al., 2015; Lu et al., 2019) show a wide range of $L \in [300, 3000]$ km and $B_n \sim (0.03, 0.3)B_0$, where B_0 is the magnetic field magnitude at the current sheet boundary. Thus, the range of the electron adiabaticity parameter $\kappa_e = (B_n/B_0)\sqrt{L/\rho_e} \in [0.1, 10]$ for the thermal electron gyroradius ρ_e (Artemyev et al., 2016). Because this parameter controls the efficiency of curvature scattering (the diffusion rate is $\sim \exp(-\kappa_e^2)$ see Birmingham (1984)), we should observe magnetized (adiabatic) electrons with weak scattering frequently. Eshetu et al. (2018, 2019) showed that low-frequency magnetic field fluctuations can locally reduce B_n and significantly enhance electron scattering and precipitation. This is one of the most promising explanations for the observed strong electron losses that are shown here with rather conservative estimates from the observed current sheets.

6 Conclusions

We investigate thermal electron spectra in Earth's magnetotail by combining a simple model of electron convection and losses with an analysis of simultaneous observations of these spectra at different distances from Earth. The main results in the study are:

1. Adiabatic electron heating caused by convection can result in a clear increase in energetic (> 1 keV) electron fluxes. This increase, however, is much weaker than predicted from pure adiabatic heating, implying that additional energetic electron losses should be taken into account to describe the observed electron spectra.
2. The estimated electron losses are comparable to losses at the strong diffusion limit, i.e., electron scattering should keep the loss cone full almost all the time during electron convection in the middle tail. Moreover, for a not-so-small convection electric field (i.e., for not-so-slow convection), the expected losses would exceed the strong diffusion limit, indicative of a widened loss cone possibly due to electron field-aligned acceleration within the auroral acceleration region.

Acknowledgments

The authors would like to thank the THEMIS instrument teams for excellent data that have been downloaded from `http://themis.ssl.berkeley.edu,respectively`. Data analysis was done using SPEDAS V3.1, see Angelopoulos et al. (2019).

Work is supported by Russian Science Foundation grant 17-72-20134 (Pavel Shustov, Alexandr Lukin), NASA contract NAS5-02099 (Anton Artemyev, Xiao-Jia Zhang, Vassilis Angelopoulos), NASA Project No. 80NSSC19K0844,and NSF Project No. 1902699 (Anton Artemyev),

References

Angelopoulos, V. (2008, December). The THEMIS Mission. *Space Sci. Rev.*, *141*, 5-34. doi: 10.1007/s11214-008-9336-1

Angelopoulos, V., Cruce, P., Drozdov, A., Grimes, E. W., Hatzigeorgiu, N., King, D. A., ... Schroeder, P. (2019, January). The Space Physics Environment Data Analysis System (SPEDAS). *Space Sci. Rev.*, *215*, 9. doi: 10.1007/s11214-018-0576-4

Angelopoulos, V., Kennel, C. F., Coroniti, F. V., Pellat, R., Spence, H. E., Kivelson, M. G., ... Gosling, J. T. (1993, August). Characteristics of ion flow in the quiet state of the inner plasma sheet. *Geophys. Res. Lett.*, *20*, 1711-1714. doi: 10.1029/93GL00847

Angelopoulos, V., McFadden, J. P., Larson, D., Carlson, C. W., Mende, S. B., Frey, H., ... Kepko, L. (2008, August). Tail Reconnection Triggering Substorm Onset. *Science*, *321*, 931-935. doi: 10.1126/science.1160495

Artemyev, A. V., Angelopoulos, V., & Runov, A. (2016, May). On the radial force balance in the quiet time magnetotail current sheet. *J. Geophys. Res.*, *121*, 4017-4026. doi: 10.1002/2016JA022480

Artemyev, A. V., Angelopoulos, V., Vasko, I. Y., Petrukovich, A. A., Runov, A., Saito, Y., ... Strangeway, R. J. (2020). Contribution of anisotropic electron current to the magnetotail current sheet as a function of location and plasma conditions. *Journal of Geophysical Research: Space Physics*, *125*(1), e2019JA027251. Retrieved from `https://agupubs.onlinelibrary.wiley.com/doi/abs/10.1029/2019JA027251` (e2019JA027251 10.1029/2019JA027251) doi: 10.1029/2019JA027251

Artemyev, A. V., Petrukovich, A. A., Nakamura, R., & Zelenyi, L. M. (2011). Clus-

ter statistics of thin current sheets in the Earth magnetotail: specifics of the dawn flank, proton temperature profiles and electrostatic effects. *J. Geophys. Res.*, *116*, A0923. doi: 10.1029/2011JA016801

Artemyev, A. V., Petrukovich, A. A., Nakamura, R., & Zelenyi, L. M. (2012). Adiabatic electron heating in the magnetotail current sheet: Cluster observations and analytical models. *J. Geophys. Res.*, *117*, A06219. doi: 10.1029/2012JA017513

Artemyev, A. V., Petrukovich, A. A., Nakamura, R., & Zelenyi, L. M. (2013, June). Profiles of electron temperature and B_z along Earth's magnetotail. *Annales Geophysicae*, *31*, 1109-1114. doi: 10.5194/angeo-31-1109-2013

Artemyev, A. V., Rankin, R., & Blanco, M. (2015, December). Electron trapping and acceleration by kinetic Alfven waves in the inner magnetosphere. *J. Geophys. Res.*, *120*, 10. doi: 10.1002/2015JA021781

Artemyev, A. V., Walsh, A. P., Petrukovich, A. A., Baumjohann, W., Nakamura, R., & Fazakerley, A. N. (2014, September). Electron pitch angle/energy distribution in the magnetotail. *J. Geophys. Res.*, *119*, 7214-7227. doi: 10.1002/2014JA020350

Artemyev, A. V., Zelenyi, L. M., Petrukovich, A. A., & Nakamura, R. (2011, July). Hot electrons as tracers of large-scale structure of magnetotail current sheets. *Geophys. Res. Lett.*, *38*, L14102. doi: 10.1029/2011GL047979

Artemyev, A. V., Zhang, X. J., Angelopoulos, V., Runov, A., Spence, H. E., & Larsen, B. A. (2018, Jul). Plasma Anisotropies and Currents in the Near-Earth Plasma Sheet and Inner Magnetosphere. *Journal of Geophysical Research (Space Physics)*, *123*(7), 5625-5639. doi: 10.1029/2018JA025232

Asano, Y., Nakamura, R., Shinohara, I., Fujimoto, M., Takada, T., Baumjohann, W., ... RèMe, H. (2008, January). Electron flat-top distributions around the magnetic reconnection region. *J. Geophys. Res.*, *113*, 1207. doi: 10.1029/2007JA012461

Ashour-Abdalla, M., El-Alaoui, M., Goldstein, M. L., Zhou, M., Schriver, D., Richard, R., ... Hwang, K.-J. (2011, April). Observations and simulations of non-local acceleration of electrons in magnetotail magnetic reconnection events. *Nature Physics*, *7*, 360-365. doi: 10.1038/nphys1903

Auster, H. U., Glassmeier, K. H., Magnes, W., Aydogar, O., Baumjohann, W., Constantinescu, D., ... Wiedemann, M. (2008, December). The THEMIS Fluxgate Magnetometer. *Space Sci. Rev.*, *141*, 235-264. doi: 10.1007/s11214-008-9365-9

Baker, D. N., Pulkkinen, T. I., Angelopoulos, V., Baumjohann, W., & McPherron, R. L. (1996, June). Neutral line model of substorms: Past results and present view. *J. Geophys. Res.*, *101*, 12975-13010. doi: 10.1029/95JA03753

Balikhin, M. A., Gedalin, M., Reeves, G. D., Boynton, R. J., & Billings, S. A. (2012, October). Time scaling of the electron flux increase at GEO: The local energy diffusion model vs observations. *J. Geophys. Res.*, *117*, 10208. doi: 10.1029/2012JA018114

Birmingham, T. J. (1984, May). Pitch angle diffusion in the Jovian magnetodisc. *J. Geophys. Res.*, *89*, 2699-2707. doi: 10.1029/JA089iA05p02699

Birn, J., Artemyev, A. V., Baker, D. N., Echim, M., Hoshino, M., & Zelenyi, L. M. (2012). Particle acceleration in the magnetotail and aurora. *Space Sci. Rev.*, *173*, 49-102. doi: 10.1007/s11214-012-9874-4

Birn, J., Hesse, M., Nakamura, R., & Zaharia, S. (2013, May). Particle acceleration in dipolarization events. *J. Geophys. Res.*, *118*, 1960-1971. doi: 10.1002/jgra.50132

Breuillard, H., Le Contel, O., Retino, A., Chasapis, A., Chust, T., Mirioni, L., ... Nakamura, R. (2016, July). Multispacecraft analysis of dipolarization fronts and associated whistler wave emissions using MMS data. *Geophys. Res. Lett.*, *43*, 7279-7286. doi: 10.1002/2016GL069188

Büchner, J., & Zelenyi, L. M. (1989, September). Regular and chaotic charged particle motion in magnetotaillike field reversals. I - Basic theory of trapped motion. *J. Geophys. Res.*, *94*, 11821-11842. doi: 10.1029/JA094iA09p11821

Chaston, C. C., Bonnell, J. W., Clausen, L., & Angelopoulos, V. (2012, September). Energy transport by kinetic-scale electromagnetic waves in fast plasma sheet flows. *J. Geophys. Res.*, *117*, 9202. doi: 10.1029/2012JA017863

Chaston, C. C., Bonnell, J. W., Peticolas, L. M., Carlson, C. W., McFadden, J. P., & Ergun, R. E. (2002, June). Driven Alfven waves and electron acceleration: A FAST case study. *Geophys. Res. Lett.*, *29*, 1535. doi: 10.1029/2001GL013842

Chaston, C. C., Peticolas, L. M., Carlson, C. W., McFadden, J. P., Mozer, F., Wilber, M., ... Balogh, A. (2005, February). Energy deposition by Alfvén waves into the dayside auroral oval: Cluster and FAST observations. *J. Geophys. Res.*, *110*, 2211. doi: 10.1029/2004JA010483

Christon, S. P., Williams, D. J., Mitchell, D. G., Huang, C. Y., & Frank, L. A. (1991, January). Spectral characteristics of plasma sheet ion and electron populations during disturbed geomagnetic conditions. *J. Geophys. Res.*, *96*, 1-22. doi: 10.1029/90JA01633

Damiano, P. A., Johnson, J. R., & Chaston, C. C. (2015, July). Ion temperature effects on magnetotail Alfvén wave propagation and electron energization. *J. Geophys. Res.*, *120*, 5623-5632. doi: 10.1002/2015JA021074

Damiano, P. A., Johnson, J. R., & Chaston, C. C. (2016). Ion gyroradius effects on particle trapping in kinetic alfvn waves along auroral field lines. *J. Geophys. Res.*, *121*(11), 10,831–10,844. Retrieved from `http://dx.doi.org/10.1002/2016JA022566` doi: 10.1002/2016JA022566

Deng, X., Ashour-Abdalla, M., Zhou, M., Walker, R., El-Alaoui, M., Angelopoulos, V., ... Schriver, D. (2010, September). Wave and particle characteristics of earthward electron injections associated with dipolarization fronts. *J. Geophys. Res.*, *115*, A09225. doi: 10.1029/2009JA015107

Dombeck, J., Cattell, C., Prasad, N., Meeker, E., Hanson, E., & McFadden, J. (2018, December). Identification of Auroral Electron Precipitation Mechanism Combinations and Their Relationships to Net Downgoing Energy and Number Flux. *J. Geophys. Res.*, *123*, 10. doi: 10.1029/2018JA025749

Echim, M. M., Maggiolo, R., Roth, M., & De Keyser, J. (2009, June). A magnetospheric generator driving ion and electron acceleration and electric currents in a discrete auroral arc observed by Cluster and DMSP. *Geophys. Res. Lett.*, *36*(12), L12111. doi: 10.1029/2009GL038343

Egedal, J., Daughton, W., & Le, A. (2012, April). Large-scale electron acceleration by parallel electric fields during magnetic reconnection. *Nature Physics*, *8*, 321-324. doi: 10.1038/nphys2249

El-Alaoui, M., Ashour-Abdalla, M., Bosqued, J. M., & Richard, R. L. (2008). Understanding magnetotail current sheet meso-scale structures using MHD simulations. *Advances in Space Research*, *41*, 1630-1642. doi: 10.1016/j.asr.2007.05.061

Ergun, R. E., Andersson, L., Main, D., Su, Y. J., Newman, D. L., Goldman, M. V., ... Mozer, F. S. (2004, December). Auroral particle acceleration by strong double layers: The upward current region. *Journal of Geophysical Research (Space Physics)*, *109*(A12), A12220. doi: 10.1029/2004JA010545

Ergun, R. E., Andersson, L., Main, D. S., Su, Y. J., Carlson, C. W., McFadden, J. P., & Mozer, F. S. (2002, September). Parallel electric fields in the upward current region of the aurora: Indirect and direct observations. *Physics of Plasmas*, *9*(9), 3685-3694. doi: 10.1063/1.1499120

Eshetu, W. W., Lyon, J. G., Hudson, M. K., & Wiltberger, M. J. (2018, November). Pitch Angle Scattering of Energetic Electrons by BBFs. *Journal of Geophysical Research (Space Physics)*, *123*(11), 9265-9274. doi: 10.1029/2018JA025788

Eshetu, W. W., Lyon, J. G., Hudson, M. K., & Wiltberger, M. J. (2019, February). Simulations of Electron Energization and Injection by BBFs Using High-Resolution LFM MHD Fields. *Journal of Geophysical Research (Space Physics)*, *124*(2), 1222-1238. doi: 10.1029/2018JA025789

Fujimoto, M., Terasawa, T., Mukai, T., Saito, Y., Yamamoto, T., & Kokubun, S. (1998, March). Plasma entry from the flanks of the near-Earth magnetotail: Geotail observations. *J. Geophys. Res.*, *103*, 4391-4408. doi: 10.1029/97JA03340

Gabrielse, C., Angelopoulos, V., Harris, C., Artemyev, A., Kepko, L., & Runov, A. (2017, May). Extensive electron transport and energization via multiple, localized dipolarizing flux bundles. *J. Geophys. Res.*, *122*, 5059-5076. doi: 10.1002/2017JA023981

Gabrielse, C., Angelopoulos, V., Runov, A., & Turner, D. L. (2012, October). The effects of transient, localized electric fields on equatorial electron acceleration and transport toward the inner magnetosphere. *J. Geophys. Res.*, *117*, 10213. doi: 10.1029/2012JA017873

Gabrielse, C., Angelopoulos, V., Runov, A., & Turner, D. L. (2014, April). Statistical characteristics of particle injections throughout the equatorial magnetotail. *J. Geophys. Res.*, *119*, 2512-2535. doi: 10.1002/2013JA019638

Gabrielse, C., Spanswick, E., Artemyev, A., Nishimura, Y., Runov, A., Lyons, L., ... Donovan, E. (2019, Jul). Utilizing the Heliophysics/Geospace System Observatory to Understand Particle Injections: Their Scale Sizes and Propagation Directions. *Journal of Geophysical Research (Space Physics)*, *124*(7), 5584-5609. doi: 10.1029/2018JA025588

Ganushkina, N. Y., Amariutei, O. A., Shprits, Y. Y., & Liemohn, M. W. (2013, January). Transport of the plasma sheet electrons to the geostationary distances. *J. Geophys. Res.*, *118*, 82-98. doi: 10.1029/2012JA017923

Ganushkina, N. Y., Amariutei, O. A., Welling, D., & Heynderickx, D. (2015, January). Nowcast model for low-energy electrons in the inner magnetosphere. *Space Weather*, *13*, 16-34. doi: 10.1002/2014SW001098

Ganushkina, N. Y., Liemohn, M. W., Amariutei, O. A., & Pitchford, D. (2014, January). Low-energy electrons (5-50 keV) in the inner magnetosphere. *J. Geophys. Res.*, *119*, 246-259. doi: 10.1002/2013JA019304

Genestreti, K. J., Fuselier, S. A., Goldstein, J., & Nagai, T. (2013). An empirical model for the location and occurrence rate of near-Earth magnetotail reconnection. *J. Geophys. Res.*, *118*, 6389-6396. doi: 10.1002/2013JA019125

Horne, R. B., Thorne, R. M., Glauert, S. A., Albert, J. M., Meredith, N. P., & Anderson, R. R. (2005, March). Timescale for radiation belt electron acceleration by whistler mode chorus waves. *J. Geophys. Res.*, *110*, 3225. doi: 10.1029/2004JA010811

Imada, S., Hirai, M., Hoshino, M., & Mukai, T. (2011, August). Favorable conditions for energetic electron acceleration during magnetic reconnection in the Earth's magnetotail. *J. Geophys. Res.*, *116*, 8217. doi: 10.1029/2011JA016576

Jaynes, A. N., Baker, D. N., Singer, H. J., Rodriguez, J. V., Loto'aniu, T. M., Ali, A. F., ... Reeves, G. D. (2015, September). Source and seed populations for relativistic electrons: Their roles in radiation belt changes. *Journal of Geophysical Research (Space Physics)*, *120*(9), 7240-7254. doi: 10.1002/2015JA021234

Keiling, A., Angelopoulos, V., Runov, A., Weygand, J., Apatenkov, S. V., Mende, S., ... Auster, H. U. (2009, May). Substorm current wedge driven by plasma flow vortices: THEMIS observations. *J. Geophys. Res.*, *114*, A00C22. doi: 10.1029/2009JA014114

Kennel, C. F. (1969). Consequences of a magnetospheric plasma. *Reviews of Geophysics and Space Physics*, *7*, 379-419. doi: 10.1029/RG007i001p00379

Khazanov, G. V., Glocer, A., & Himwich, E. W. (2014, Jan). Magnetosphere-ionosphere energy interchange in the electron diffuse aurora. *Journal of Geophysical Research (Space Physics)*, *119*(1), 171-184. doi: 10.1002/2013JA019325

Khazanov, G. V., Robinson, R. M., Zesta, E., Sibeck, D. G., Chu, M., & Grubbs, G. A. (2018, July). Impact of Precipitating Electrons and Magnetosphere-Ionosphere Coupling Processes on Ionospheric Conductance. *Space Weather*, *16*(7), 829-837. doi: 10.1029/2018SW001837

Khazanov, G. V., Shen, Y., Vasko, I. Y., Artemyev, A. V., & Chu, M. (2021, May). Magnetosphere Ionosphere Coupling of Precipitated Electrons in Diffuse Aurora Driven by Time Domain Structures. *Geophys. Res. Lett.*, *48*(10), e92655. doi: 10.1029/2021GL092655

Khazanov, G. V., Sibeck, D. G., & Zesta, E. (2017, Apr). Major pathways to electron distribution function formation in regions of diffuse aurora. *Journal of Geophysical Research (Space Physics)*, *122*(4), 4251-4265. doi: 10.1002/2017JA023956

Kiehas, S. A., Runov, A., Angelopolos, V., Hietala, H., & Korovinksiy, D. (2018, March). Magnetotail Fast Flow Occurrence Rate and Dawn-Dusk Asymmetry at $X_{GSM} \sim -60$ R_E. *J. Geophys. Res.*, *123*, 1767-1778. doi: 10.1002/2017JA024776

Kivelson, M. G., & Spence, H. E. (1988, December). On the possibility of quasi-static convection in the quiet magnetotail. *Geophys. Res. Lett.*, *15*, 1541-1544. doi: 10.1029/GL015i013p01541

Knetter, T., Neubauer, F. M., Horbury, T., & Balogh, A. (2004, June). Four-point discontinuity observations using Cluster magnetic field data: A statistical survey. *J. Geophys. Res.*, *109*, A06102. doi: 10.1029/2003JA010099

Li, B., Marklund, G., Alm, L., Karlsson, T., Lindqvist, P. A., & Masson, A. (2014, November). Statistical altitude distribution of Cluster auroral electric fields, indicating mainly quasi-static acceleration below 2.8 R_E and Alfvénic above. *Journal of Geophysical Research (Space Physics)*, *119*(11), 8984-8991. doi: 10.1002/2014JA020225

Liang, J., Ni, B., Cully, C. M., Donovan, E. F., Thorne, R. M., & Angelopoulos, V. (2012, March). Electromagnetic ELF wave intensification associated with fast earthward flows in mid-tail plasma sheet. *Annales Geophysicae*, *30*, 467-488. doi: 10.5194/angeo-30-467-2012

Liang, J., Spanswick, E., Nicolls, M. J., Donovan, E. F., Lummerzheim, D., & Liu, W. W. (2011, June). Multi-instrument observations of soft electron precipitation and its association with magnetospheric flows. *J. Geophys. Res.*, *116*, 6201. doi: 10.1029/2010JA015867

Liu, J., Angelopoulos, V., Kubyshkina, M., McFadden, J., Glassmeier, K.-H., & Russell, C. T. (2011, May). Revised timing and onset location of two isolated substorms observed by Time History of Events and Macroscale Interactions During Substorms (THEMIS). *J. Geophys. Res.*, *116*, 0. doi: 10.1029/2010JA015877

Lu, S., Artemyev, A. V., Angelopoulos, V., Lin, Y., Zhang, X. J., Liu, J., ... Strangeway, R. J. (2019, Feb). The Hall Electric Field in Earth's Magnetotail Thin Current Sheet. *Journal of Geophysical Research (Space Physics)*, *124*(2), 1052-1062. doi: 10.1029/2018JA026202

Lyons, L. R. (1984, July). Electron energization in the geomagnetic tail current sheet. *J. Geophys. Res.*, *89*, 5479-5487. doi: 10.1029/JA089iA07p05479

Lysak, R. L. (1990, February). Electrodynamic coupling of the magnetosphere and ionosphere. *Space Sci. Rev.*, *52*, 33-87. doi: 10.1007/BF00704239

Lysak, R. L., & Song, Y. (2011, September). Development of parallel electric fields at the plasma sheet boundary layer. *J. Geophys. Res.*, *116*, A00K14. doi: 10.1029/2010JA016424

Ma, Q., Connor, H. K., Zhang, X. J., Li, W., Shen, X. C., Gillespie, D., ... Spence, H. E. (2020, August). Global Survey of Plasma Sheet Electron Precipitation due to Whistler Mode Chorus Waves in Earth's Magnetosphere. *Geophys. Res. Lett.*, *47*(15), e88798. doi: 10.1029/2020GL088798

Malaspina, D. M., Wygant, J. R., Ergun, R. E., Reeves, G. D., Skoug, R. M., & Larsen, B. A. (2015). Electric field structures and waves at plasma boundaries in the inner magnetosphere. *J. Geophys. Res.*, *120*, n/a–n/a. (2015JA021137) doi: 10.1002/2015JA021137

McFadden, J. P., Carlson, C. W., Larson, D., Ludlam, M., Abiad, R., Elliott, B., ... Angelopoulos, V. (2008, December). The THEMIS ESA Plasma Instrument and In-flight Calibration. *Space Sci. Rev.*, *141*, 277-302. doi: 10.1007/s11214-008-9440-2

Mozer, F. S., Agapitov, O., Artemyev, A., Drake, J. F., Krasnoselskikh, V., Lejosne, S., & Vasko, I. (2015). Time domain structures: What and where they are, what they do, and how they are made. *Geophys. Res. Lett.*, *42*, 3627-3638. doi: 10.1002/2015GL063946

Mozer, F. S., Cattell, C. A., Hudson, M. K., Lysak, R. L., Temerin, M., & Torbert, R. B. (1980, October). Satellite measurements and theories of low altitude auroral particle acceleration. *Space Sci. Rev.*, *27*(2), 155-213. doi: 10.1007/BF00212238

Mozer, F. S., & Kletzing, C. A. (1998, January). Direct observation of large, quasi-static, parallel electric fields in the auroral acceleration region. *Geophys. Res. Lett.*, *25*(10), 1629-1632. doi: 10.1029/98GL00849

Nagai, T., Zenitani, S., Shinohara, I., Nakamura, R., Fujimoto, M., Saito, Y., & Mukai, T. (2013, December). Ion and electron dynamics in the ion-electron decoupling region of magnetic reconnection with Geotail observations. *J. Geophys. Res.*, *118*, 7703-7713. doi: 10.1002/2013JA019135

Nakamura, R., Baumjohann, W., Runov, A., & Asano, Y. (2006, February). Thin Current Sheets in the Magnetotail Observed by Cluster. *Space Science Reviews*, *122*, 29-38. doi: 10.1007/s11214-006-6219-1

Newell, P. T., Sotirelis, T., & Wing, S. (2009, September). Diffuse, monoenergetic, and broadband aurora: The global precipitation budget. *J. Geophys. Res.*, *114*, A09207. doi: 10.1029/2009JA014326

Newell, P. T., Sotirelis, T., & Wing, S. (2010, March). Seasonal variations in diffuse, monoenergetic, and broadband aurora. *Journal of Geophysical Research (Space Physics)*, *115*(A3), A03216. doi: 10.1029/2009JA014805

Ni, B., Liang, J., Thorne, R. M., Angelopoulos, V., Horne, R. B., Kubyshkina, M., ... Lummerzheim, D. (2012, January). Efficient diffuse auroral electron scattering by electrostatic electron cyclotron harmonic waves in the outer magnetosphere: A detailed case study. *J. Geophys. Res.*, *117*, 1218. doi: 10.1029/2011JA017095

Ni, B., Thorne, R. M., Horne, R. B., Meredith, N. P., Shprits, Y. Y., Chen, L., & Li, W. (2011, April). Resonant scattering of plasma sheet electrons leading to diffuse auroral precipitation: 1. Evaluation for electrostatic electron cyclotron harmonic waves. *J. Geophys. Res.*, *116*, 4218. doi: 10.1029/2010JA016232

Ni, B., Thorne, R. M., Meredith, N. P., Horne, R. B., & Shprits, Y. Y. (2011, April). Resonant scattering of plasma sheet electrons leading to diffuse auroral precipitation: 2. Evaluation for whistler mode chorus waves. *J. Geophys. Res.*, *116*, 4219. doi: 10.1029/2010JA016233

Ni, B., Thorne, R. M., Shprits, Y. Y., Orlova, K. G., & Meredith, N. P. (2011, June). Chorus-driven resonant scattering of diffuse auroral electrons in nondipolar magnetic fields. *J. Geophys. Res.*, *116*, 6225. doi: 10.1029/2011JA016453

Ni, B., Thorne, R. M., Zhang, X., Bortnik, J., Pu, Z., Xie, L., ... Gu, X. (2016, April). Origins of the Earth's Diffuse Auroral Precipitation. *Space Sci. Rev.*,

200, 205-259. doi: 10.1007/s11214-016-0234-7

Nishimura, Y., Lessard, M. R., Katoh, Y., Miyoshi, Y., Grono, E., Partamies, N., ... Kurita, S. (2020, January). Diffuse and Pulsating Aurora. *Space Sci. Rev.*, *216*(1), 4. doi: 10.1007/s11214-019-0629-3

Panov, E. V., Artemyev, A. V., Baumjohann, W., Nakamura, R., & Angelopoulos, V. (2013, June). Transient electron precipitation during oscillatory BBF braking: THEMIS observations and theoretical estimates. *J. Geophys. Res.*, *118*, 3065-3076. doi: 10.1002/jgra.50203

Petrukovich, A. A., Artemyev, A. V., Vasko, I. Y., Nakamura, R., & Zelenyi, L. M. (2015). Current sheets in the Earth magnetotail: plasma and magnetic field structure with Cluster project observations. *Space Sci. Rev.*, *188*, 311-337. doi: 10.1007/s11214-014-0126-7

Petrukovich, A. A., Baumjohann, W., Nakamura, R., & Rème, H. (2009, September). Tailward and earthward flow onsets observed by Cluster in a thin current sheet. *J. Geophys. Res.*, *114*, 9203. doi: 10.1029/2009JA014064

Rankin, R., Samson, J. C., & Tikhonchuk, V. T. (1999). Parallel electric fields in dispersive shear Alfvén waves in the dipolar magnetosphere. *Geophys. Res. Lett.*, *26*, 3601-3604. doi: 10.1029/1999GL010715

Runov, A., Angelopoulos, V., Gabrielse, C., Liu, J., Turner, D. L., & Zhou, X.-Z. (2015, June). Average thermodynamic and spectral properties of plasma in and around dipolarizing flux bundles. *J. Geophys. Res.*, *120*, 4369-4383. doi: 10.1002/2015JA021166

Runov, A., Angelopoulos, V., Sitnov, M. I., Sergeev, V. A., Bonnell, J., McFadden, J. P., ... Auster, U. (2009, July). THEMIS observations of an earthward-propagating dipolarization front. *Geophys. Res. Lett.*, *36*, L14106. doi: 10.1029/2009GL038980

Runov, A., Angelopoulos, V., Zhou, X.-Z., Zhang, X.-J., Li, S., Plaschke, F., & Bonnell, J. (2011, May). A THEMIS multicase study of dipolarization fronts in the magnetotail plasma sheet. *J. Geophys. Res.*, *116*, 5216. doi: 10.1029/2010JA016316

Runov, A., Sergeev, V. A., Nakamura, R., Baumjohann, W., Apatenkov, S., Asano, Y., ... Balogh, A. (2006, March). Local structure of the magnetotail current sheet: 2001 Cluster observations. *Annales Geophysicae*, *24*, 247-262.

Sarafopoulos, D. V., Sidiropoulos, N. F., Sarris, E. T., Lutsenko, V., & Kudela, K. (2001, July). The dawn-dusk plasma sheet asymmetry of energetic particles: An interball perspective. *J. Geophys. Res.*, *106*, 13053-13066. doi: 10.1029/2000JA900157

Sergeev, V. A., Baumjohann, W., & Shiokawa, K. (2001). Bi-directional electron distributions associated with near-tail flux transport. *Geophys. Res. Lett.*, *28*, 3813-3816. doi: 10.1029/2001GL013334

Sergeev, V. A., Pellinen, R. J., & Pulkkinen, T. I. (1996, February). Steady Magnetospheric Convection: A Review of Recent Results. *Space Sci. Rev.*, *75*, 551-604. doi: 10.1007/BF00833344

Sergeev, V. A., Sormakov, D. A., Apatenkov, S. V., Baumjohann, W., Nakamura, R., Runov, A. V., ... Nagai, T. (2006, August). Survey of large-amplitude flapping motions in the midtail current sheet. *Annales Geophysicae*, *24*, 2015-2024.

Shen, Y., Artemyev, A., Zhang, X.-J., Vasko, I. Y., Runov, A., Angelopoulos, V., & Knudsen, D. (2020, August). Potential Evidence of Low-Energy Electron Scattering and Ionospheric Precipitation by Time Domain Structures. *Geophys. Res. Lett.*, *47*(16), e89138. doi: 10.1029/2020GL089138

Stiles, G. S., Hones, E. W., Jr., Bame, S. J., & Asbridge, J. R. (1978, July). Plasma sheet pressure anisotropies. *J. Geophys. Res.*, *83*, 3166-3172. doi: 10.1029/JA083iA07p03166

Tao, X., Thorne, R. M., Li, W., Ni, B., Meredith, N. P., & Horne, R. B. (2011,

April). Evolution of electron pitch angle distributions following injection from the plasma sheet. *J. Geophys. Res.*, *116*, A04229. doi: 10.1029/2010JA016245

Tikhonchuk, V. T., & Rankin, R. (2002, July). Parallel potential driven by a kinetic Alfvén wave on geomagnetic field lines. *J. Geophys. Res.*, *107*, 1104. doi: 10.1029/2001JA000231

Tsyganenko, N. A. (1995, April). Modeling the Earth's magnetospheric magnetic field confined within a realistic magnetopause. *J. Geophys. Res.*, *100*, 5599-5612. doi: 10.1029/94JA03193

Tsyganenko, N. A. (2002, August). A model of the near magnetosphere with a dawn-dusk asymmetry 1. Mathematical structure. *J. Geophys. Res.*, *107*, 1179. doi: 10.1029/2001JA000219

Tsyganenko, N. A., & Sitnov, M. I. (2005, March). Modeling the dynamics of the inner magnetosphere during strong geomagnetic storms. *J. Geophys. Res.*, *110*, A03208. doi: 10.1029/2004JA010798

Tverskoy, B. A. (1969). Main mechanisms in the formation of the Earth's radiation belts. *Reviews of Geophysics and Space Physics*, *7*, 219-231. doi: 10.1029/RG007i001p00219

Vasko, I. Y., Agapitov, O. V., Mozer, F. S., Artemyev, A. V., Krasnoselskikh, V. V., & Bonnell, J. W. (2017, March). Diffusive scattering of electrons by electron holes around injection fronts. *J. Geophys. Res.*, *122*, 3163-3182. doi: 10.1002/2016JA023337

Vasko, I. Y., Krasnoselskikh, V. V., Mozer, F. S., & Artemyev, A. V. (2018, July). Scattering by the broadband electrostatic turbulence in the space plasma. *Physics of Plasmas*, *25*(7), 072903. doi: 10.1063/1.5039687

Vasko, I. Y., Petrukovich, A. A., Artemyev, A. V., Nakamura, R., & Zelenyi, L. M. (2015, October). Earth's distant magnetotail current sheet near and beyond lunar orbit. *J. Geophys. Res.*, *120*, 8663-8680. doi: 10.1002/2015JA021633

Volwerk, M., Baumjohann, W., Glassmeier, K., Nakamura, R., Zhang, T., Runov, A., ... Rème, H. (2004, January). Compressional waves in the Earth's neutral sheet. *Annales Geophysicae*, *22*, 303-315. doi: 10.5194/angeo-22-303-2004

Walsh, A. P., Fazakerley, A. N., Forsyth, C., Owen, C. J., Taylor, M. G. G. T., & Rae, I. J. (2013). Sources of electron pitch angle anisotropy in the magnetotail plasma sheet. *J. Geophys. Res.*, *118*, 6042–6054. doi: 10.1002/jgra.50553

Walsh, A. P., Owen, C. J., Fazakerley, A. N., Forsyth, C., & Dandouras, I. (2011, March). Average magnetotail electron and proton pitch angle distributions from Cluster PEACE and CIS observations. *Geophys. Res. Lett.*, *38*, 6103. doi: 10.1029/2011GL046770

Wang, C., Lyons, L. R., Wolf, R. A., Nagai, T., Weygand, J. M., & Lui, A. T. Y. (2009, April). Plasma sheet $PV^{5/3}$ and nV and associated plasma and energy transport for different convection strengths and AE levels. *J. Geophys. Res.*, *114*, A00D02. doi: 10.1029/2008JA013849

Wygant, J. R., Keiling, A., Cattell, C. A., Lysak, R. L., Temerin, M., Mozer, F. S., ... Russell, C. T. (2002, August). Evidence for kinetic Alfvén waves and parallel electron energization at 4-6 R_E altitudes in the plasma sheet boundary layer. *J. Geophys. Res.*, *107*, 1201. doi: 10.1029/2001JA900113

Zelenyi, L. M., Zogin, D. V., & Büchner, J. (1990). Quasiadiabatic dynamics of charged particles in the tail of the magnetosphere. *Cosmic Research*, *28*, 369-380.

Zhang, X., & Angelopoulos, V. (2014, April). On the relationship of electrostatic cyclotron harmonic emissions with electron injections and dipolarization fronts. *J. Geophys. Res.*, *119*, 2536-2549. doi: 10.1002/2013JA019540

Zhang, X., Angelopoulos, V., Artemyev, A. V., & Liu, J. (2018, September). Whistler and Electron Firehose Instability Control of Electron Distributions in and Around Dipolarizing Flux Bundles. *Geophys. Res. Lett.*, *45*, 9380-9389.

807 doi: 10.1029/2018GL079613
808 Zhang, X., Angelopoulos, V., Ni, B., Thorne, R. M., & Horne, R. B. (2014, July).
809 Extent of ECH wave emissions in the Earth's magnetotail. *J. Geophys. Res.*,
810 *119*, 5561-5574. doi: 10.1002/2014JA019931
811 Zhang, X.-J., Angelopoulos, V., Ni, B., & Thorne, R. M. (2015, January). Predom-
812 inance of ECH wave contribution to diffuse aurora in Earth's outer magneto-
813 sphere. *J. Geophys. Res.*, *120*, 295-309. doi: 10.1002/2014JA020455